Original Article

Palovarotene inhibits osteochondroma formation in a mouse model of multiple hereditary exostoses[†]

Toshihiro Inubushi,[1] Isabelle Lemire,[2] Fumitoshi Irie,[1] and Yu Yamaguchi[1]

[1]Human Genetics Program, Sanford Burnham Prebys Medical Discovery Institute, 10901 North Torrey Pines Road, La Jolla, CA 92037, USA.

[2]Clementia Pharmaceuticals Inc., 4150 Ste-Catherine Street West, Suite 550, Montreal, Qc, H3Z 2Y5, Canada.

Correspondence author: Yu Yamaguchi, Sanford Burnham Prebys Medical Discovery Institute, 10901 North Torrey Pines Road, La Jolla, CA 92037, USA. Phone: 858-646-3124; Fax: 858-646-3197; e-mail: yyamaguchi@sbpdiscovery.org

[†]This article has been accepted for publication and undergone full peer review but has not been through the copyediting, typesetting, pagination and proofreading process, which may lead to differences between this version and the Version of Record. Please cite this article as doi: [10.1002/jbmr.3341]

Additional Supporting Information may be found in the online version of this article.

Initial Date Submitted September 8, 2017; Date Revision Submitted November 6, 2017; Date Final Disposition Set November 8, 2017

Journal of Bone and Mineral Research

DOI 10.1002/jbmr.3341

Abstract

Multiple hereditary exostoses (MHE), also known as multiple osteochondromas (MO), is an autosomal dominant disorder characterized by the development of multiple cartilage-capped bone tumors (osteochondromas). The large majority of patients with MHE carry loss-of-function mutations in the *EXT1* or *EXT2* gene, which encodes a glycosyltransferase essential for heparan sulfate (HS) biosynthesis. Increasing evidence suggests that enhanced BMP signaling resulting from loss of HS expression plays a role in osteochondroma formation in MHE. Palovarotene (PVO) is a retinoic acid receptor γ selective agonist, which is being investigated as a potential drug for fibrodysplasia ossificans progressiva (FOP), another genetic bone disorder with features that overlap with those of MHE. Here we show that PVO inhibits osteochondroma formation in the $Fsp1^{Cre};Ext1^{flox/flox}$ model of MHE. Four-week daily treatment with PVO starting at postnatal day (P) 14 reduced the number of osteochondromas that develop in these mice by up to 91% in a dose-dependent manner. An inhibition of long bone growth observed in animals treated from P14 was almost entirely abrogated by delaying the initiation of treatment to P21. We also found that PVO attenuates BMP signaling in $Fsp1^{Cre};Ext1^{flox/flox}$ mice, and that aberrant chondrogenic fate determination of *Ext1*-deficient perichondrial progenitor cells in these mice is restored by PVO. Together, the present data support further preclinical and clinical investigations of PVO as a potential therapeutic agent for MHE.

Key Words: Multiple hereditary exostosis (MHE); Multiple osteochondromas (MO); Palovarotene, EXT1, Heparan sulfate

This article is protected by copyright. All rights reserved

Introduction

Multiple hereditary exostoses (MHE; OMIM 133700/133701), also called multiple osteochondromas (MO), is a rare genetic bone disorder characterized by the development of numerous benign bone tumors (osteochondromas) with an estimated prevalence of at least 1 in 50,000 (1, 2). The majority (~90%) of patients with MHE carry heterozygous loss-of-function mutations of *EXT1* or *EXT2* genes (1). EXT1 and EXT2 are essential for the biosynthesis of heparan sulfate (HS), a sulfate glycosaminoglycan. EXT1 is a glycosyltransferase catalyzing the elongation of HS chains, whereas EXT2 acts as a chaperone for EXT1 (3). HS plays physiological roles in diverse developmental processes by modulating function of various growth factors and morphogens (4), with endochondral ossification being one such developmental process in which HS plays a particularly important role (5, 6). Accumulating evidence suggests that aberrantly enhanced BMP signaling, resulting from the loss of HS expression in mesenchymal progenitor cells in the perichondrium, is the key molecular culprit underlying osteochondroma formation in MHE (7-9).

Although osteochondromas themselves are not malignant, they can cause a variety of skeletal problems, including bone deformity and shortening, malalignment, and limitation of joint mobility (10). Osteochondromas also tend to impinge on and compress soft tissue and nerves, causing local and generalized pain (11). Moreover, there is a small but not negligible risk of malignant transformation into chondrosarcoma and other sarcomas (1). Due to these problems, patients with MHE often require multiple surgeries to remove osteochondromas and to correct bone deformity such as limb-length inequalities and malalignment (12). Currently, surgical resection of existing osteochondromas is essentially the only treatment for MHE (13).

Toward the development of pharmacological therapy for MHE, we and others have previously reported that LDN-193189, a BMP type I receptor inhibitor (14), reduces osteochondroma formation in MHE mouse models (8, 9). In this paper, we test another potential drug for MHE, palovarotene (PVO). PVO is a retinoic acid receptor γ (RARγ) selective agonist that was originally in development as a possible drug for emphysema (15). A phase 2 clinical trial based on this indication has demonstrated the excellent safety profile of PVO (16). In 2011, Shimono et al. (17) reported that RARγ selective agonists, including PVO, are potent inhibitors of heterotopic ossification, suggesting potential therapeutic benefits of PVO in fibrodysplasia ossificans progressiva (FOP), a rare genetic disease characterized by heterotopic ossification (18). FOP is caused by an activating mutation in the BMP type I receptor ACVR1 (also known as ALK2) (19) and chemical inhibitors of BMP type I receptor signaling reduce heterotopic ossification (20). Although the mechanism of action by which PVO reduces heterotopic ossification has not been completely elucidated, it is mediated, at least partly, by inhibition of BMP signaling (17).

While the prevalence and clinical phenotype are quite distinct, MHE and FOP share several phenotypic and mechanistic similarities. For example, FOP patients tend to develop MHE-like osteochondromas (21). Mechanistically, FOP is caused by constitutive activation of BMP signaling, while excessive BMP signaling due to loss of HS is a contributing factor for osteochondroma formation (7-9). These observations led us to hypothesize that PVO might inhibit osteochondroma formation in MHE. Here we show the results of a preclinical study to test the efficacy of PVO on osteochondroma formation in a mouse model of MHE. Our results

demonstrate that PVO is a remarkably potent inhibitor of osteochondroma formation. Our results also suggest that this activity of PVO is mediated by restoring the normal pattern of fate determination of perichondrial progenitor cells via attenuation of BMP signaling.

Materials and Methods

Mice

Perichondrium-targeted conditional *Ext1* knockout mice (*Fsp1^{Cre};Ext1$^{flox/flox}$*) were generated by crossing mice carrying the *Ext1^{flox}* allele (22) and the *Fsp1^{Cre}* transgene (23). *Rosa26-tdTomato* (*R26^{tdTomato}*) mice (24) were obtained from The Jackson Laboratory (Bar Harbor, ME; Stock No: 007909). Genotyping of the mice was performed by PCR as described previously (8, 25). All mouse lines used in this study were in 100% C57Bl/6J background. Animals were housed in solid-bottom, microisolater cages in ventilated racks under a 12 h light/dark cycle and fed standard laboratory chow (Irradiated 2018 Teklad Global 18%Protein Rodent Diet, Envigo Laboratories) *ad libitum*. All animal procedures were performed in accordance with NIH *Guide for the care and use of Laboratory Animals* and approved by the IACUC of the Sanford Burnham Prebys Medical Discovery Institute.

Drug treatment

Mice: Fsp1^{Cre};Ext1$^{flox/flox}$ mice used in this study were produced from 25 mating pairs of *Fsp1^{Cre};Ext1$^{flox/+}$* male and *Ext1$^{flox/flox}$* female mice. Offspring from these mating pairs were genotyped using tail DNA by PCR at postnatal day (P) 7. We conducted two PVO treatment experiments that differed in the timing and duration of treatment. In Experiment 1, mice received daily oral gavage of PVO starting at P14 for 4 weeks (P14–42), while in Experiment 2, mice

received daily oral gavage starting at P21 for 3 weeks (P21–42). In both experiments, four groups of mice were given either 1.76, 0.88, 0.27, or 0 (vehicle control) mg/kg/day of PVO. Upon genotyping, *Fsp1*^{Cre}*;Ext1*$^{flox/flox}$ mice were randomized using the random number calculator of GraphPad software and assigned to the above treatment groups according to the randomization list. The number of mice assigned to these experimental groups is described in Supplementary Table 1. There were no animal deaths during the treatment period (found dead or euthanized for humane reasons) in any of the experimental arms. Two mice were initially assigned but subsequently excluded from data analysis due to an incorrect determination of genotype. One mouse was excluded due to an incorrect treatment protocol applied to it during the study.

Palovarotene administration: Dosing formulations of PVO were prepared by Clementia Pharmaceuticals Inc. (Montreal, Canada) and shipped to the Yamaguchi laboratory frozen as ready-to-use daily coded aliquots, which were kept at –20˚C until use. Dosing formulations of PVO (0.0449, 1.47, and 2.94 mg/ml) were prepared by diluting a stock solution of PVO (10 mg/ml in DMSO) with corn oil. The control dosing formulation (vehicle) was 2.94% DMSO in corn oil. On the day of dosing, the appropriate number of aliquots was removed from the freezer and allowed to thaw at room temperature. Daily dosing of PVO or vehicle was performed by oral gavage. The dose volume was set at 6 ml/kg and based on the body weight measurement of each animal just prior to dosing. The oral doses were given to conscious, non-anesthetized animals using a syringe with attached gavage cannula. Personnel performing these procedures were blinded to the identity of the formulation throughout the drug treatment period. During the course of the experiment, mice were monitored daily for signs of distress, including general conditions and behavior.

Analysis of mice: At the end of the treatment period, mice were sacrificed and genotyped again to confirm the genotypes. Carcasses were processed for whole-mount skeletal preparations, in which the number of osteochondromas and other bone phenotypes were examined. Briefly, under a stereoscopic microscope, discrete protrusions with alcian blue-positive cartilage cap were identified and their number was counted in 12 ribs (the 1st rib bone was excluded from the analysis) and in five major limb long bones (ulna, radius, humerus, femur, tibia) of the right hemi-skeleton. Longitudinal lengths were measured for the ulna, radius, humerus, femur, and tibia using ImageJ processing of microphotographs taken with a CCD camera.

Whole-mount skeletal preparation, histology, and immunohistochemistry

Whole-mount skeletal preparations were prepared as described previously (8). For histology and immunohistochemistry, tissue specimens were fixed in 4% paraformaldehyde in PBS, decalcified in EDTA, and frozen in SCEM compound (Section-Lab, Hiroshima, Japan). The cut surface was covered with an adhesive film (Cryofilm type IIC9, Section-Lab, Japan) and sections (5 μm) were cut with a microtome (CM3050 Leica Microsystems, Germany) (8). For Safranin O staining, frozen sections were stained in 0.02% aqueous Fast Green, rinsed in 1% acetic acid, and stained with 0.1% aqueous Safranin O. For immunostaining, frozen sections were blocked with PBS containing 5% donkey serum and 0.3% Triton X-100. Sections were then incubated overnight at 4˚C with primary antibodies, followed by detection with secondary antibodies at dilutions recommended by manufacturers. Nuclei were stained by 4',6-diamidino-2-phenylindole (DAPI; Invitrogen, Eugene OR). For staining with the anti-type II collagen, sections were pre-treated with hyaluronidase (2 U/ml; Sigma-Aldrich) for 2 h at 37˚C. Antibodies used in immunohistochemistry were: mouse monoclonal anti-type II collagen (Cat. No. ab54236) and rat

polyclonal anti-CD44 (Cat. No. ab25340) from Abcam (Cambridge, MA); rabbit polyclonal anti-phospho-Smad1/5/8 (Cat. No. AB3848) from EMD Millipore (Temecula, CA); Alexa 488-labelled donkey anti-rabbit IgG (Cat. No. 711-545-152), Alexa 488-labelled donkey anti-mouse IgG (Cat. No. 715-545-151), and Alexa 488-labelled donkey anti-rat IgG (Cat. No. 712-545-153) from Jackson ImmunoResearch Laboratories (West Grove, PA).

BrdU labeling

Mice were injected with BrdU (0.1 mg/g, i.p.), sacrificed 3 h later, and sections of bones were prepared as described above. After treatment with 0.1% trypsin (for 1 h at 37˚C) and 1 N hydrochloric acid (for 30 min at 37˚C), sections were stained with rat monoclonal anti-BrdU antibody (Cat. No. GTX26326; Gene Tex, San Antonio, TX) and DAPI. The ratio of proliferating cells was determined by dividing the number of $BrdU^+$ cells by the number of DAPI-stained nuclei in the proliferative zone of the growth plate and in the cartilage cap of osteochondromas.

Cell culture and Western blotting

Isolation of perichondrial mesenchymal progenitor cells (PDPCs) from *Ext1*$^{flox/flox}$ mice and *in vitro* ablation of *Ext1* by Cre-IRES-Puro lentivirus were described previously (8). Western blotting was performed with rabbit polyclonal anti-phospho-Smad1/5/8 antibody (described above), rabbit polyclonal anti-Smad1/5/8 (Cat. No. sc-6031-R) from Santa Cruz Biotechnology (Dallas, TX), and mouse monoclonal anti-α-tubulin antibody (Cat. No. T6074) from Sigma-Aldrich (St. Louis, MO).

Statistical analysis

Statistical methods were not used to predetermine sample size. Statistical analyses were performed with GraphPad Prism 7. Unpaired student's two-sided *t* test with Welch's correction, one-way ANOVA and two-way ANOVA were used under the assumption of normal distribution and observance of similar variance. Bonferroni post hoc analysis was performed where applicable. Values are expressed as means. In all experiments, inter-group variances were similar and data were symmetrically distributed. Data shown are representative images; each analysis was performed on at least three mice per genotype. Immunostaining was performed at least in triplicate. For other experiments, the numbers of biological replicates, animals, or cells are indicated in the text. Images shown are representative of the entire data set.

Results

Validation of the *Fsp1^{Cre};Ext1$^{flox/flox}$* model for preclinical testing of PVO.

There are several mouse models for MHE. *Ext1*$^{+/-}$ and *Ext2*$^{+/-}$ mice recapitulate human MHE genotypes, but they develop osteochondromas in less than 30% of animals (26, 27), far lower than the nearly complete penetrance of osteochondroma formation in human MHE (1). Moreover, unlike human MHE, these heterozygous mice develop osteochondromas only in rib bones (26). *Ext1*$^{+/-}$;*Ext2*$^{+/-}$ compound heterozygotes develop osteochondromas in long bones as well as in rib bones, while the penetrance of osteochondroma formation is still not complete (28). In contrast, conditional knockout mouse models targeted to chondrocytes (25, 29) and perichondrial cells (8) develop multiple osteochondromas both in long and rib bones at 100% penetrance. For this study, we used the *Fsp1^{Cre};Ext1$^{flox/flox}$* perichondrium-targeted conditional knockout model (8), which not only develop multiple osteochondromas at 100% penetrance but

also grow normally and survive more than 1 year (8). These features make *Fsp1^{Cre};Ext1$^{flox/flox}$* mice excellent hosts for long-term drug treatment studies.

Generation and characterization of *Fsp1^{Cre};Ext1$^{flox/flox}$* mice have been reported (8). For this study, we performed additional characterization to further validate the model for use in the PVO treatment study. First, the time course of osteochondroma development was analyzed in *Fsp1^{Cre};Ext1$^{flox/flox}$* mice (Supplementary Fig. S1). At P14, no osteochondromas were observed in either the femur or ribs. Ectopic clusters of chondrocytes, which are thought to be the "seeds" of osteochondromas, were first detected at around P21. By P42, *Fsp1^{Cre};Ext1$^{flox/flox}$* mice exhibit full-blown osteochondroma formation. Second, we ascertained that PVO treatment does not alter the efficiency or spatial pattern of *Fsp1^{Cre}*-mediated recombination using the *R26^{tdTomato}* reporter gene (24). *Fsp1^{Cre};R26^{tdTomato}* mice were treated daily with 1.76 mg/kg of PVO or vehicle from P21 to P42. There were no differences in the number and distribution of tdTomato^{+} cells between PVO- and vehicle-treated *Fsp1^{Cre};R26^{tdTomato}* mice (Supplementary Fig. S2), confirming the validity of this model for the PVO treatment experiments.

PVO treatment inhibits osteochondroma formation.

In the first set of experiment (Experiment 1), *Fsp1^{Cre};Ext1$^{flox/flox}$* mice were treated with PVO daily from P14 to P42. Four groups of *Fsp1^{Cre};Ext1$^{flox/flox}$* mice were given daily oral gavage of 0.27 ("low dose"), 0.88 ("medium dose"), 1.76 ("high dose") mg/kg of PVO, or vehicle ("vehicle") (Fig. 1A–1D). In this cohort, there were no animal deaths during the treatment period (found dead or euthanized for humane reasons). In the vehicle-treated group, the total number of osteochondromas in five major limb long bones (humerus, radius, ulna, femur, and tibia) was

58.5±8.2. In comparison, the numbers of long bone osteochondromas in the low, medium, and high dose groups were 25.3±3.4 (56.8% reduction), 9.0±3.3 (84.6% reduction), and 5.2±1.1 (91.1% reduction), respectively (Fig. 1A). The number of osteochondromas in ribs was similarly reduced by PVO in a dose dependent manner (Fig. 1B). (Actual data on the number of osteochondromas and the length of limb bones are presented in Supplementary Table 1.) Representative images depicting osteochondromas in these groups are shown in Fig. 1I. While the inhibitory effect on osteochondroma formation was remarkable, PVO treatment also inhibited the longitudinal growth of long bones by up to 21.8% in the high and medium dose groups (Fig. 1C and 1D; Supplementary Table 1) in this protocol starting at P14.

A previous study reported that PVO administered to 1-month old FOP mice does not inhibit bone growth (30), suggesting that the observed effect on long bone growth is dependent on the age of mice. To determine if delaying the initiation of PVO treatment can alleviate the inhibitory effect, a second experiment was performed using PVO treatment from P21 to P42 (Experiment 2). As in the first cohort, there were no animal deaths during the treatment period. With this delayed protocol, the total number of osteochondromas in the five long bones was still significantly reduced by 32.0%, 67.8%, and 88.4% in low, medium, and high dose groups, respectively (Fig. 1E). The total number of osteochondromas in ribs was similarly reduced by PVO (Fig. 1F). Remarkably, with delayed PVO administration, there were no differences in the length of long bones (Fig. 1G and 1H; Supplementary Table 1). Together, the results from these two drug treatment experiments demonstrate that PVO has a significant effect in suppressing osteochondroma formation in *Fsp1*^{Cre}*;Ext1*$^{flox/flox}$ mice, and that the inhibitory effect of PVO on bone growth can be alleviated by delaying the initiation of treatment.

Analysis of PVO effects at the histological level.

Sections of femurs and ribs from the high-dose group of Experiment 2 (1.76 mg/kg/day, P21–P42) were analyzed at the histological level on P42 for the effect of PVO. Safranin O staining reveals numerous ectopic clusters of chondrocytes as well as overgrowth of growth plate cartilage in vehicle-treated *Fsp1*^{Cre};*Ext1*$^{flox/flox}$ mice (Fig. 2C and 2G). In comparison, PVO-treated *Fsp1*^{Cre};*Ext1*$^{flox/flox}$ mice are largely free of osteochondromas both in long and rib bones (Fig. 2D and 2H), although ectopic clusters of chondrocytes were occasionally found in the perichondrium and periosteum (*arrowheads*). In addition, PVO treatment appears to have a normalizing effect on the growth plate. In vehicle-treated *Fsp1*^{Cre};*Ext1*$^{flox/flox}$ mice, the growth plate has a wavy appearance with irregular thickness (Fig. 2C; *CKO/Vehicle* in Fig. 2I). In PVO-treated *Fsp1*^{Cre};*Ext1*$^{flox/flox}$ mice, the normal structural organization of the growth plate is partially restored (Fig. 2D; *CKO/PVO* in Fig. 2I). Of note, PVO does not have adverse effect on the growth plate in WT mice (Fig. 2B, *WT/PVO* in Fig. 2I).

We also examined the effect of PVO on chondrocyte proliferation in the growth plate and osteochondromas using a BrdU incorporation assay. The percentage of BrdU^{+} cells relative to the total DAPI^{+} nuclei was not different between vehicle-treated and PVO-treated groups either in the growth plate or in the cartilage cap of osteochondromas (Fig. 2J), suggesting that PVO's osteochondroma-suppressive effect is not due to the inhibition of chondrocytes proliferation.

PVO rectifies aberrant differentiation of *Ext1*-deficient progenitor cells.

We previously reported that *Ext1*-deficient progenitor cells in the perichondrium undergo

aberrant differentiation into chondrocytes, and that these ectopic chondrocytes serve as seeds of osteochondromas (8). To examine the possibility that PVO modulates this process, we analyzed the early phase of osteochondroma development by fate mapping. For this purpose, we generated *Fsp1*^{Cre};*R26*^{tdTomato};*Ext1*$^{flox/flox}$ triple compound mice, which were treated with PVO (1.76 mg/kg/day) or vehicle and analyzed for the behavior of tdTomato^{+} cells. As a reference, vehicle-treated *Fsp1*^{Cre};*R26*^{tdTomato} (i.e., no *Ext1* ablation) mice were also analyzed in the same manner.

In ribs of the reference mice (Fig. 3A), tdTomato^{+} cells (which are *Ext1*$^{+/+}$) were seen in the perichondrium, periosteum, and bone trabeculae, with good colocalization of tdTomato and CD44 signals. In contrast, tdTomato and type II collagen (Col2) signals showed essentially no colocalization. Since CD44 marks mesenchymal stem cells (MSCs) and cells of the osteoblastic lineage in developing bones (31), these results indicate that wild-type (*Ext1*$^{+/+}$) progenitor cells maintain the property of MSCs, and that their progeny primarily differentiate along the osteoblastic lineage. In *Fsp1*^{Cre};*R26*^{tdTomato};*Ext1*$^{flox/flox}$ mice (Fig. 3B), on the other hand, tdTomato^{+} cells were observed within ectopic clusters of chondrocytes (*arrowheads*), with little colocalization between tdTomato and CD44 signals in the perichondrium and periosteum. This suggests that progenitor cells lacking *Ext1* alter their fate and form ectopic chondrocyte clusters in the perichondrium and periosteum. This observation is further supported by the colocalization of tdTomato and Col2 signals in these ectopic chondrocyte clusters (Fig. 3B).

Effects of PVO on this aberrant fate determination were analyzed in *Fsp1*^{Cre};*R26*^{tdTomato};*Ext1*$^{flox/flox}$ mice treated by PVO. Here, the distribution of tdTomato^{+} cells was largely reversed compared to that seen in reference mice, and the colocalization of tdTomato

and CD44 signals was restored (Fig. 3C). These results indicate that PVO has the effect of rectifying the aberrant fate determination of *Ext1*-deficient progenitor cells during the early phase of osteochondroma development.

PVO attenuates enhanced BMP signaling in *Ext1*-deficient perichondrial cells.

While PVO, as an agonist of retinoid signaling, potentially regulates multiple pathways, it has been suggested that the inhibitory effect of PVO on heterotopic ossification is mediated by the attenuation of BMP signaling (17). In addition, increasing evidence in mice indicates that osteochondroma formation is mediated by enhanced BMP signaling in mesenchymal progenitor cells in the perichondrium (7-9). Therefore, we asked whether PVO modulates BMP signaling in $Fsp1^{Cre};R26^{tdTomato};Ext1^{flox/flox}$ mice (The $R26^{tdTomato}$ reporter gene is included in these mice to confirm the occurrence of recombination). Immunostaining of ribs with anti-phospho-Smad1/5/8 (pSmad1/5/8) antibody, a probe for canonical BMP signaling, revealed that pSmad1/5/8 immunoreactivity is increased both in the perichondrium and periosteum in vehicle-treated $Fsp1^{Cre};R26^{tdTomato};Ext1^{flox/flox}$ mice (*CKO/Vehicle* in Fig. 4A and 4B), consistent with our previous finding (8). On the other hand, in PVO-treated $Fsp1^{Cre};R26^{tdTomato};Ext1^{flox/flox}$ mice, pSmad1/5/8 immunoreactivity was significantly reduced to a level similar to that seen in wild-type mice (*CKO/PVO* in Fig. 4A and 4B), indicating that PVO does attenuate enhanced BMP signaling in the *Ext1*-deficient perichondrium/periosteum. This observation was further corroborated by *in vitro* analysis using primary cultures of perichondrium-derived mesenchymal progenitor cells (PDPCs) (8). As shown in Fig. 4C, BMP2-mediated Smad1/5/8 phosphorylation was attenuated by PVO treatment both in wild-type and *Ext1*-deficient PDPCs. Together, these results demonstrate that PVO inhibits BMP signaling in mesenchymal progenitor cells in the

perichondrium. This suggests that the osteochondroma-suppressive effect of PVO is at least partly attributable to its attenuation of the enhanced BMP signaling that occurs in *Ext1*-deficient cells.

Discussion

This study investigated whether PVO has the ability to inhibit osteochondroma formation in a mouse model of MHE. PVO has been shown to suppress heterotopic ossification in mouse models of FOP, an effect that is mediated, at least partly, by attenuation of excessive BMP signaling due to constitutively active mutations of the BMP receptor ACVR1 (17, 32, 33). Since increasing evidence suggests that enhanced BMP signaling also contributes to osteochondroma formation in MHE mouse models (7-9), we postulate that PVO could suppress osteochondroma formation in MHE. This study demonstrates that PVO is a potent inhibitor of osteochondroma formation in the $Fsp1^{Cre};Ext1^{flox/flox}$ model of MHE.

We have previously reported that treatment with the small molecule BMP inhibitor LDN-193189 suppresses osteochondroma formation in $Fsp1^{Cre};Ext1^{flox/flox}$ mice (8), the same model used in this study. It is noteworthy that the osteochondroma-suppressive effect of orally administered PVO is substantially greater than that of LDN-193189 administered intraperitoneally. For example, our previous study showed that the number of rib osteochondromas in $Fsp1^{Cre};Ext1^{flox/flox}$ mice was reduced by 52.5% with 10 mg/kg/day LDN-193189, i.p. for 4 weeks (P14–P42) (8). In comparison, 0.88 mg/kg/day PVO, p.o. during the same period reduced the number of rib osteochondromas by 81.8% (see Supplementary Table 1). Although it is possible that the dose of LDN-193189 used in the previous study was suboptimal, the effect of PVO

nevertheless appears remarkable in comparison. It remains to be determined why PVO is more potent than the inhibitor that specifically targets BMP signaling. It is possible that PVO also acts on a non-BMP pathway(s) that influence fate determination of perichondrial progenitor cells. The possible toxicity and side effects of PVO in humans has been characterized extensively, which indicates that PVO is generally well tolerated in both healthy volunteers and patients with emphysema (15). Our current results also show that PVO exerts little adverse effect on the overall health of mice. Together, these observations suggest that PVO possesses more favorable features than LDN-193189 as a therapeutic and/or preventive agent for human MHE.

Our results demonstrate that PVO inhibits the longitudinal growth of long bones when treatment is initiated at P14 at the medium and high doses (Fig. 1C and 1D). This observation is consistent with known effects of retinoic acid on the developing skeleton (34). Interestingly, this inhibitory effect is almost entirely abrogated by delaying the initiation of treatment to P21 (Fig. 1G and 1H). This suggests the presence of a "critical period" for the emergence of this adverse effect of PVO, and that once past this period, PVO does not affect long bone growth. Consistent with this notion, it has been reported that PVO administered to 1-month old FOP mice does not inhibit bone growth (30). Therefore, the timing and dosage of PVO intervention would be important considerations in the further development of PVO as a possible therapy for MHE.

Although elucidation of the mechanism of action by which PVO suppresses osteochondroma formation is not a primary goal of this study, our data provide some insight into this issue. First, our fate mapping analysis revealed a striking effect of PVO to rectify aberrant chondrogenic fate determination of *Ext1*-deficient progenitor cells (Fig. 3), whereas PVO does not show

appreciable inhibitory effects on cell proliferation (Fig. 2J). This suggests that PVO's osteochondroma-suppressive activity is mediated primarily by its effect on fate determination of progenitor cells, rather than an effect on the proliferation of chondrocytes. The observed effect of PVO to suppress chondrogenic fate determination appears to be in line with the previous report that RARγ agonists suppress chondrogenic differentiation of cultured limb mesenchymal cells (17). Second, we found that PVO attenuates BMP signaling in *Ext1*-deficient perichondrial progenitor cells *in vivo* and *in vitro* (Fig. 4). As mentioned above, inhibition of BMP signaling with LDN-193189 has been shown to suppress osteochondroma formation in three different MHE mouse models (8, 9). Thus, although PVO likely modulates multiple pathways, not limited to the canonical BMP pathway, it seems fair to speculate that the osteochondroma-suppressive effect of PVO is mediated mainly by its inhibitory effect on BMP signaling. In this context, it is interesting that retinoic acid has been shown to reduce BMP signaling via degradation of phosphorylated Smad1 in mouse embryonic carcinoma cells (35). It remains to be determined whether PVO attenuates BMP signaling by this mechanism.

In conclusion, this study presents evidence that PVO suppresses osteochondroma formation in a mouse model of MHE. While there remain several unresolved issues, such as the efficacy in different mouse models and the effect on preexisting osteochondromas, we believe that these data support further preclinical and clinical investigations of PVO as a potential therapeutic agent for MHE.

Acknowledgements

This work was supported by National Institutes of Health Grant R01AR055670 and a grant from Clementia Pharmaceuticals (to Y.Y.). T.I. was the recipient of a Postdoctoral Fellowship for Research Abroad from Japan Society for the Promotion of Science. We thank Dr. Eric Neilson (Vanderbilt University) for providing *Fsp1*^{Cre} mice; Adriana Charbono for helping animal care and oral gavage procedures; Mao Inubushi for technical support; and the MHE Research Foundation for support and encouragement.

Author's roles: Y.Y. and I.L. conceived the study. T.I., I.L., and Y.Y. designed the experiments. T.I. and F.I. performed experiments and analyzed data. I.L. assisted in analysis of data. T.I. and Y.Y. wrote the paper.

Disclosures

Y.Y. is a recipient of a research grant from and a consultant of Clementia Pharmaceuticals. I.L. is an employee of Clementia Pharmaceuticals and hold stock/stock options in the company. All other authors state that they have no conflicts of interest.

References

1. Wuyts W, Schmale GA, Chansky HA, and Raskind WH. In: Pagon RA, Adam MP, Ardinger HH, Wallace SE, Amemiya A, Bean LJH, Bird TD, Ledbetter N, Mefford HC, Smith RJH, et al. eds. *GeneReviews(R)*. Seattle (WA); 2013.
2. Schmale GA, Conrad EU, 3rd, and Raskind WH. The natural history of hereditary multiple exostoses. *J Bone Joint Surg Am.* 1994;76(7):986-92.
3. Senay C, Lind T, Muguruma K, Tone Y, Kitagawa H, Sugahara K, Lidholt K, Lindahl U, and Kusche-Gullberg M. The EXT1/EXT2 tumor suppressors: catalytic activities and role in heparan sulfate biosynthesis. *EMBO reports.* 2000;1(3):282-6.
4. Bishop JR, Schuksz M, and Esko JD. Heparan sulphate proteoglycans fine-tune mammalian physiology. *Nature.* 2007;446(7139):1030-7.
5. Matsumoto Y, Matsumoto K, Irie F, Fukushi J, Stallcup WB, and Yamaguchi Y. Conditional ablation of the heparan sulfate-synthesizing enzyme Ext1 leads to dysregulation of bone morphogenic protein signaling and severe skeletal defects. *J Biol Chem.* 2010;285(25):19227-34.
6. Koziel L, Kunath M, Kelly OG, and Vortkamp A. Ext1-dependent heparan sulfate regulates the range of Ihh signaling during endochondral ossification. *Dev Cell.* 2004;6(6):801-13.
7. Huegel J, Mundy C, Sgariglia F, Nygren P, Billings PC, Yamaguchi Y, Koyama E, and Pacifici M. Perichondrium phenotype and border function are regulated by Ext1 and heparan sulfate in developing long bones: a mechanism likely deranged in Hereditary Multiple Exostoses. *Dev Biol.* 2013;377(1):100-12.
8. Inubushi T, Nozawa S, Matsumoto K, Irie F, and Yamaguchi Y. Aberrant perichondrial BMP signaling mediates multiple osteochondromagenesis in mice. *JCI Insight.* 2017;2(15).
9. Sinha S, Mundy C, Bechtold T, Sgariglia F, Ibrahim MM, Billings PC, Carroll K, Koyama E, Jones KB, and Pacifici M. Unsuspected osteochondroma-like outgrowths in the cranial base of Hereditary Multiple Exostoses patients and modeling and treatment with a BMP antagonist in mice. *PLoS Genet.* 2017;13(4):e1006742.
10. Stieber JR, and Dormans JP. Manifestations of hereditary multiple exostoses. *J Am Acad Orthop Surg.* 2005;13(2):110-20.
11. Darilek S, Wicklund C, Novy D, Scott A, Gambello M, Johnston D, and Hecht J. Hereditary multiple exostosis and pain. *J Pediatr Orthop.* 2005;25(3):369-76.
12. Porter DE, Lonie L, Fraser M, Dobson-Stone C, Porter JR, Monaco AP, and Simpson AH. Severity of disease and risk of malignant change in hereditary multiple exostoses. A genotype-phenotype study. *J Bone Joint Surg Br.* 2004;86(7):1041-6.
13. Kitsoulis P, Galani V, Stefanaki K, Paraskevas G, Karatzias G, Agnantis NJ, and Bai M. Osteochondromas: review of the clinical, radiological and pathological features. *In Vivo.* 2008;22(5):633-46.
14. Cuny GD, Yu PB, Laha JK, Xing X, Liu JF, Lai CS, Deng DY, Sachidanandan C, Bloch KD, and Peterson RT. Structure-activity relationship study of bone morphogenetic protein (BMP) signaling inhibitors. *Bioorg Med Chem Lett.* 2008;18(15):4388-92.
15. Hind M, and Stinchcombe S. Palovarotene, a novel retinoic acid receptor gamma agonist for the treatment of emphysema. *Curr Opin Investig Drugs.* 2009;10(11):1243-50.

16. Stolk J, Stockley RA, Stoel BC, Cooper BG, Piitulainen E, Seersholm N, Chapman KR, Burdon JG, Decramer M, Abboud RT, et al. Randomised controlled trial for emphysema with a selective agonist of the gamma-type retinoic acid receptor. *Eur Respir J.* 2012;40(2):306-12.
17. Shimono K, Tung WE, Macolino C, Chi AH, Didizian JH, Mundy C, Chandraratna RA, Mishina Y, Enomoto-Iwamoto M, Pacifici M, et al. Potent inhibition of heterotopic ossification by nuclear retinoic acid receptor-gamma agonists. *Nat Med.* 2011;17(4):454-60.
18. Shore EM, and Kaplan FS. Insights from a rare genetic disorder of extra-skeletal bone formation, fibrodysplasia ossificans progressiva (FOP). *Bone.* 2008;43(3):427-33.
19. Shore EM, Xu M, Feldman GJ, Fenstermacher DA, Cho TJ, Choi IH, Connor JM, Delai P, Glaser DL, LeMerrer M, et al. A recurrent mutation in the BMP type I receptor ACVR1 causes inherited and sporadic fibrodysplasia ossificans progressiva. *Nat Genet.* 2006;38(5):525-7.
20. Yu PB, Deng DY, Lai CS, Hong CC, Cuny GD, Bouxsein ML, Hong DW, McManus PM, Katagiri T, Sachidanandan C, et al. BMP type I receptor inhibition reduces heterotopic [corrected] ossification. *Nat Med.* 2008;14(12):1363-9.
21. Deirmengian GK, Hebela NM, O'Connell M, Glaser DL, Shore EM, and Kaplan FS. Proximal tibial osteochondromas in patients with fibrodysplasia ossificans progressiva. *J Bone Joint Surg Am.* 2008;90(2):366-74.
22. Inatani M, Irie F, Plump AS, Tessier-Lavigne M, and Yamaguchi Y. Mammalian brain morphogenesis and midline axon guidance require heparan sulfate. *Science.* 2003;302(5647):1044-6.
23. Bhowmick NA, Chytil A, Plieth D, Gorska AE, Dumont N, Shappell S, Washington MK, Neilson EG, and Moses HL. TGF-beta signaling in fibroblasts modulates the oncogenic potential of adjacent epithelia. *Science.* 2004;303(5659):848-51.
24. Madisen L, Zwingman TA, Sunkin SM, Oh SW, Zariwala HA, Gu H, Ng LL, Palmiter RD, Hawrylycz MJ, Jones AR, et al. A robust and high-throughput Cre reporting and characterization system for the whole mouse brain. *Nat Neurosci.* 2010;13(1):133-40.
25. Matsumoto K, Irie F, Mackem S, and Yamaguchi Y. A mouse model of chondrocyte-specific somatic mutation reveals a role for Ext1 loss of heterozygosity in multiple hereditary exostoses. *Proc Natl Acad Sci U S A.* 2010;107(24):10932-7.
26. Stickens D, Zak BM, Rougier N, Esko JD, and Werb Z. Mice deficient in Ext2 lack heparan sulfate and develop exostoses. *Development.* 2005;132(22):5055-68.
27. Hilton MJ, Gutierrez L, Martinez DA, and Wells DE. EXT1 regulates chondrocyte proliferation and differentiation during endochondral bone development. *Bone.* 2005;36(3):379-86.
28. Zak BM, Schuksz M, Koyama E, Mundy C, Wells DE, Yamaguchi Y, Pacifici M, and Esko JD. Compound heterozygous loss of Ext1 and Ext2 is sufficient for formation of multiple exostoses in mouse ribs and long bones. *Bone.* 2011;48(5):979-87.
29. Jones KB, Piombo V, Searby C, Kurriger G, Yang B, Grabellus F, Roughley PJ, Morcuende JA, Buckwalter JA, Capecchi MR, et al. A mouse model of osteochondromagenesis from clonal inactivation of Ext1 in chondrocytes. *Proc Natl Acad Sci U S A.* 2010;107(5):2054-9.
30. Chakkalakal SA, Uchibe K, Convente MR, Zhang D, Economides AN, Kaplan FS, Pacifici M, Iwamoto M, and Shore EM. Palovarotene Inhibits Heterotopic Ossification

and Maintains Limb Mobility and Growth in Mice With the Human ACVR1(R206H) Fibrodysplasia Ossificans Progressiva (FOP) Mutation. *J Bone Miner Res.* 2016;31(9):1666-75.

31. Jamal HH, and Aubin JE. CD44 expression in fetal rat bone: in vivo and in vitro analysis. *Exp Cell Res.* 1996;223(2):467-77.
32. Pavey GJ, Qureshi AT, Tomasino AM, Honnold CL, Bishop DK, Agarwal S, Loder S, Levi B, Pacifici M, Iwamoto M, et al. Targeted stimulation of retinoic acid receptor-gamma mitigates the formation of heterotopic ossification in an established blast-related traumatic injury model. *Bone.* 2016;90(159-67.
33. Sinha S, Uchibe K, Usami Y, Pacifici M, and Iwamoto M. Effectiveness and mode of action of a combination therapy for heterotopic ossification with a retinoid agonist and an anti-inflammatory agent. *Bone.* 2016;90(59-68.
34. Armstrong RB, Ashenfelter KO, Eckhoff C, Levin AA, and Shapiro SS. *The Retinoids: Biology, Chemistry, and Medicine*. New York: Raven Press; 1994:545-72.
35. Sheng N, Xie Z, Wang C, Bai G, Zhang K, Zhu Q, Song J, Guillemot F, Chen YG, Lin A, et al. Retinoic acid regulates bone morphogenic protein signal duration by promoting the degradation of phosphorylated Smad1. *Proc Natl Acad Sci U S A.* 2010;107(44):18886-91.

Figure legends

Figure 1. PVO suppresses osteochondroma formation in *Fsp1^{Cre};Ext1$^{flox/flox}$* mice.

Fsp1^{Cre};Ext1$^{flox/flox}$ mice were treated by daily oral gavage with 0.27, 0.88 or 1.76 mg/kg of PVO or vehicle (*Vehicle*) and the effects on osteochondroma formation and bone growth were analyzed at the end of the treatments. (***A–D***) *Fsp1^{Cre};Ext1$^{flox/flox}$* mice were treated from P14 to P42 (Experiment 1). (***E–H***) *Fsp1^{Cre};Ext1$^{flox/flox}$* mice were treated from P21 to P42 (Experiment 2). (***A*** and ***E***) The total number of osteochondromas in five major limb bones (ulna, radius, humerus, tibia, femur) of the right hemi-skeleton per animal. (***B*** and ***F***) The total number of osteochondromas in 12 ribs of the right hemi-skeleton per animal. (***C*** and ***G***) The longitudinal length of the tibia. (***D*** and ***H***) The longitudinal length of the femur. In Experiment 1, the mean number of osteochondromas in the 0.27, 0.88 or 1.76 mg/kg/day groups in comparison with the vehicle group was reduced by 56.8%, 84.6%, and 91.1%, respectively, in long bones (***A***) and by 57.5%, 81.8%, and 90.8%, respectively, in ribs (***B***). With this treatment protocol (i.e., P14–42), the longitudinal length of long bones was reduced by up to 21.8% (***C*** and ***D***). In Experiment 2, the mean number of osteochondromas in the 0.27, 0.88 or 1.76 mg/kg/day groups in comparison with the vehicle group was reduced by 32.0%, 67.8%, and 88.4%, respectively, in long bones (***E***) and by 34.1%, 54.6%, and 77.6%, respectively, in ribs (***F***). With this treatment protocol (i.e., P21–42), PVO showed no inhibitory effect on the longitudinal growth of long bones (***G*** and ***H***). See also the Supplementary Table 1 for the summary of all data from these drug treatment experiments, including the data on the ulna, radius, and humerus, which are not shown in this figure. * $p<0.05$, *** $p<0.001$ by one-way ANOVA followed by Bonferroni's post hoc test. *n.s.*, not significant. (***I***) Representative images of hindlimbs and ribs in the indicated treatment groups. Scale bars, 0.1 mm.

Figure 2. Histological assessment of the effect of PVO. *Fsp1^{Cre};Ext1$^{flox/flox}$* (*CKO*) and wild-type (*WT*) mice, treated with 1.76 mg/kg/day PVO or vehicle from P21 to P42 (Experiment 2), were histologically examined at P42. (***A*** and ***B***) Safranin O-stained sections of the femur (***A***–***D***) and the 10th rib (***E***–***H***). Right images in each panel show high-magnification images of the perichondrium (*PC*) and periosteum (*PO*). Note that there are numerous abnormal chondrocyte clusters and overgrowth of cartilage in vehicle-treated *Fsp1^{Cre};Ext1$^{flox/flox}$* mice (***C*** and ***G***). In PVO-treated *Fsp1^{Cre};Ext1$^{flox/flox}$* mice, such lesions mostly disappear (***D*** and ***H***), although there are occasional ectopic clusters of chondrocytes (*arrowheads*). (***I***) Effects of PVO on growth plate organization. Safranin O-stained sections of the distal femur growth plate reveal an irregular morphology of the growth plate and a mild disorganization of chondrocytic columnization in vehicle-treated *Fsp1^{Cre};Ext1$^{flox/flox}$* mice (*CKO/Vehicle*; see also Fig. 2C). PVO treatment partially restores the normal organization of the growth plate (*CKO/PVO*). Data shown are representative images. Each analysis was performed on at least 5 animals per genotype. (***J***) Effects of PVO on chondrocyte proliferation. After 3-week treatment with PVO or vehicle, mice at P42 were analyzed by BrdU labeling. The ratio of proliferating cells was determined by dividing the number of BrdU-positive cells by total number of DAPI-stained nuclei in the proliferating zone of the femoral growth plate (*Growth plate*; n = 5 animals/genotype/treatment) and in the cartilage cap of osteochondromas (*Osteochondroma*; n = 27 discrete osteochondromas/treatment). Means are shown as horizontal bars. Two-way ANOVA followed by Bonferroni's post hoc test was used for the growth plate data and student's *t* test for the osteochondroma data; *n.s.*, not significant. Scale bars, 0.1 mm (*A–D* and *I*); 0.2 mm (*E–H*).

Figure 3. PVO restores normal fate determination of *Ext1*-deficient progenitor cells in the perichondrium. *Fsp1*^{Cre};*R26*^{tdTomato} mice (*WT*) and *Fsp1*^{Cre};*R26*^{tdTomato};*Ext1*$^{flox/flox}$ (*CKO*) mice were treated by daily oral gavage of 1.76 mg/kg PVO or vehicle starting at P21. At P31, mice were sacrificed and frozen sections of the 10th rib were examined for the localization of tdTomato^{+} cells, which are cells that have undergone *Fsp1*^{Cre}-mediated recombination and their progeny. Sections were also stained with anti-CD44 (*CD44*) and DAPI or anti-type II collagen antibody (*Col2*) and DAPI to determine the differentiation state of tdTomato^{+} cells. Smaller images on the lower right of each panel represent high-magnification views of the perichondrium/periosteum. (***A***) *Fsp1*^{Cre};*R26*^{tdTomato} (*WT*) mice treated with vehicle. (***B***) *Fsp1*^{Cre};*R26*^{tdTomato};*Ext1*$^{flox/flox}$ (*CKO*) mice treated with vehicle. (***C***) *Fsp1*^{Cre};*R26*^{Tomato};*Ext1*$^{flox/flox}$ (*CKO*) mice treated with PVO. Note that tdTomato^{+} progenitor cells in WT mice (***A***) also express CD44 (thus *yellow* signals in the upper left image) but not Col2 (no *yellow* signals in the lower left image), which indicates that *Fsp1*-expressing progenitor cells maintain the property of progenitor cells and that their progeny contribute primarily to osteoblastic cells. In contrast, in CKO mice (***B***), *Ext1*-deficient progenitor cells contribute to Col2^{+} chondrocytes forming ectopic clusters of chondrocytes (*white arrowheads*). CKO mice treated with PVO (***C***) show reversion of tdTomato^{+} progenitor cells to the normal pattern of fate determination. Scale bars, 0.1 mm.

Figure 4. PVO attenuates enhanced BMP signaling in *Ext1*-deficient perichondrium. *Fsp1*^{Cre};*R26*^{tdTomato};*Ext1*$^{flox/flox}$ (*CKO*) mice were treated by daily oral gavage of 1.76 mg/kg PVO or vehicle for 5 days starting at P21. At P26, these mice as well as vehicle-treated *Fsp1*^{Cre};*R26*^{tdTomato} (*WT*) mice were sacrificed, and frozen sections of the 10th ribs were stained with anti-pSmad1/5/8 antibody (*green*). *Fsp1*^{Cre}-mediated recombination was monitored by

tdTomato (*red*). (***A***) pSmad1/5/8 expression in the perichondrium. (***B***) pSmad1/5/8 expression in the periosteum. Note that only low levels of pSmad1/5/8 are seen in the perichondrium and periosteum of vehicle-treated WT mice (*WT/Vehicle*), whereas Smad1/5/8 is strongly phosphorylated in vehicle-treated CKO mice (*CKO/Vehicle*). In PVO-treated CKO mice, Smad1/5/8 phosphorylation is attenuated to the WT level (*CKO/PVO*). Data shown are representative images. Each analysis was performed on at least 3 animals per genotype. Scale bars, 50 μm (***A*** and ***B***). (***C***) *Ext1*-deficient ($Ext1^{-/-}$) and wild-type (*WT*) PDPCs in monolayer cultures were pretreated with 1 μM PVO in DMSO or DMSO only for 48 h. Then, cells were incubated with 10 ng/ml BMP2 for 30 min and lysed. Cell lysates were immunoblotted with antibodies to pSmad1/5/8, total Smad1/5/8, and α-tubulin. This experiment was performed three times with similar results.

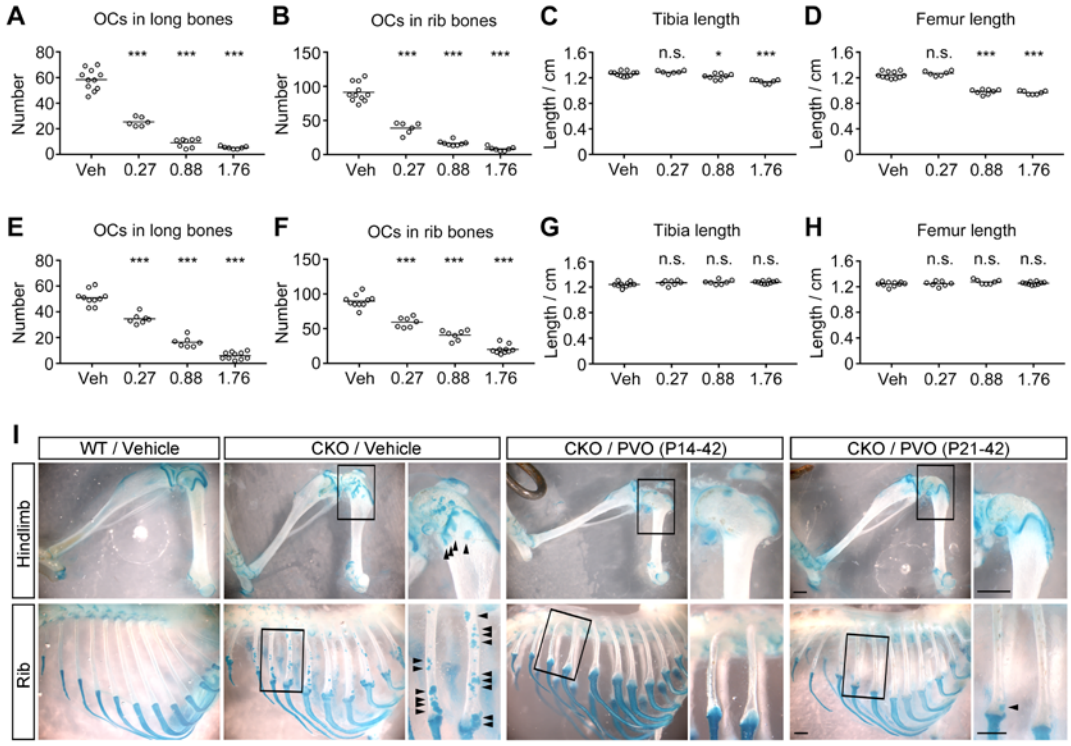

Figure 1

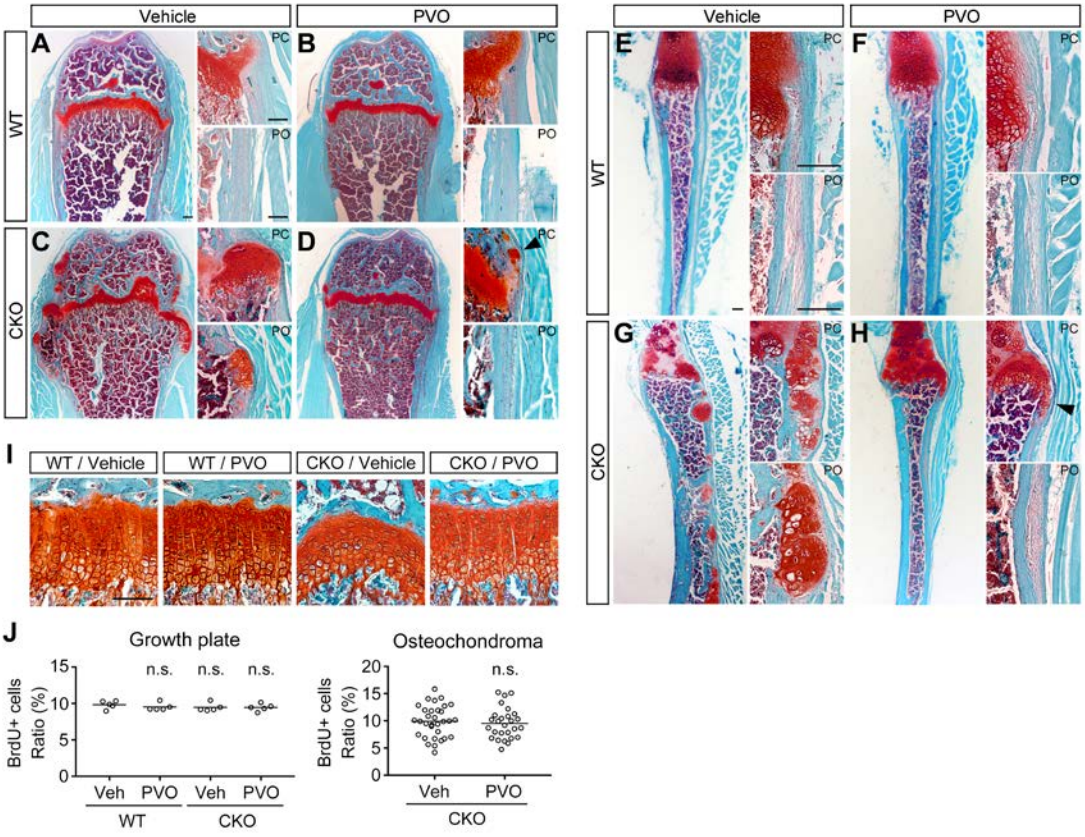

Figure 2

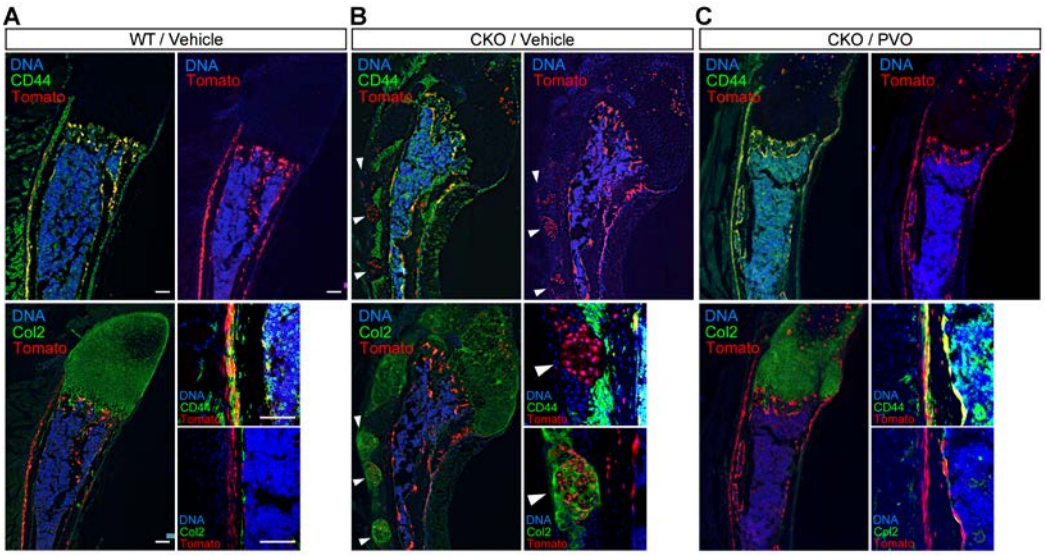

Figure 3

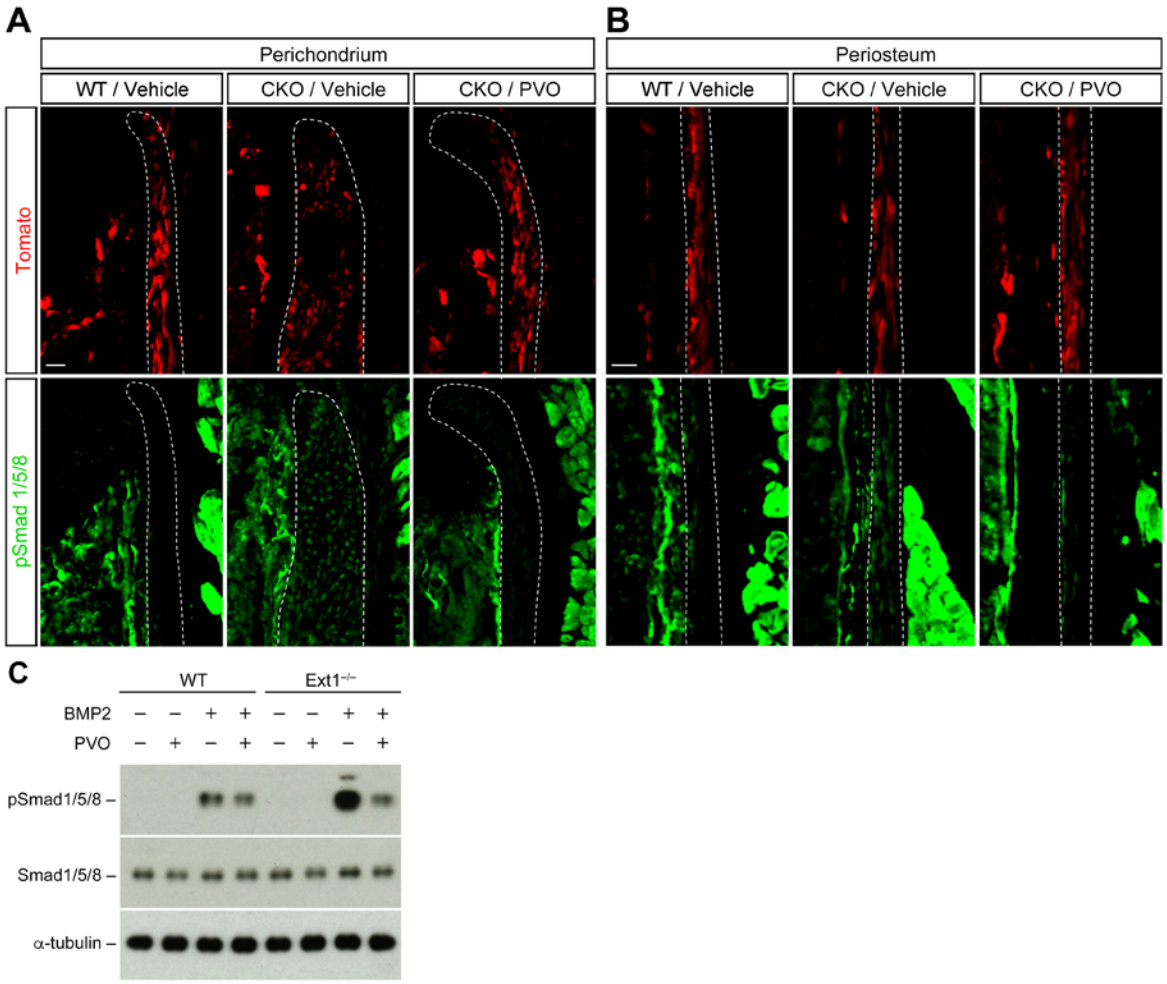

Figure 4